Report on an

ELECTRICAL GEOPHYSICAL SURVEY IN THE VICINITY OF KELEY HOT SPRINGS, MODOC COUNTY, CALIFORNIA

conducted by

ROBERT B. FURGERSON
Consulting Geophysicist
717 Oak Street, Suite 5
Lakewood, Colorado 80215
(303) 237-9732

under contract to

GEOTHERMAL POWER CORP.
160 Samsone, Suite 1201
San Francisco, California 94104

November 16, 1973

Introduction

This report describes the results obtained from an electrical geophysical survey carried out in the vicinity of Kelly Hot Springs, California, during October, 1973 by Robert B. Furgerson under contract to Geothermal Power Corp. The objective of the survey was to outline areas of anomalously conductive ground which may be associated with geothermal activity for the purpose of locating drilling sites to test the potential for geothermal power production from the prospect. The area surveyed lies in Modoc County, in northesat California approximately 17 miles west of Alturas and immediately east of Canby on Highway 299 (see Figure 1 for location map). The survey area is covered by the Alturas, California, topographic map of the U.S. Geological Survey at a scale of 1:62,500.

General Geology and Structure

The survey area lies in the geomorphic province known as the Modoc Plateau and is characterized by extensive Tertiary and Quaternary lava flows, volcanoes, and cinder cones. These volcanic rocks overlie lake and stream sediments of Pliocene age, known as the Alturas Formation (Gay, 1959, p. 6). The province is broken by northwest- and north-trending normal faults that divide the volcanic surface into blocks, with intervening sediment-filled basins. Plutonic and metamorphic rocks probably underlie the volcanic rocks throughout much of the area (MacDonald, 1966, p. 65).

The Tertiary and Quaternary volcanic rocks found throughout most of the area include many broad-spreading "plateau" lava flows and pyroclastic deposits that range in composition from basalt to rhyolite and in age from Oligocene to Recent. Associated with the volcanic rocks in many areas are nonmarine

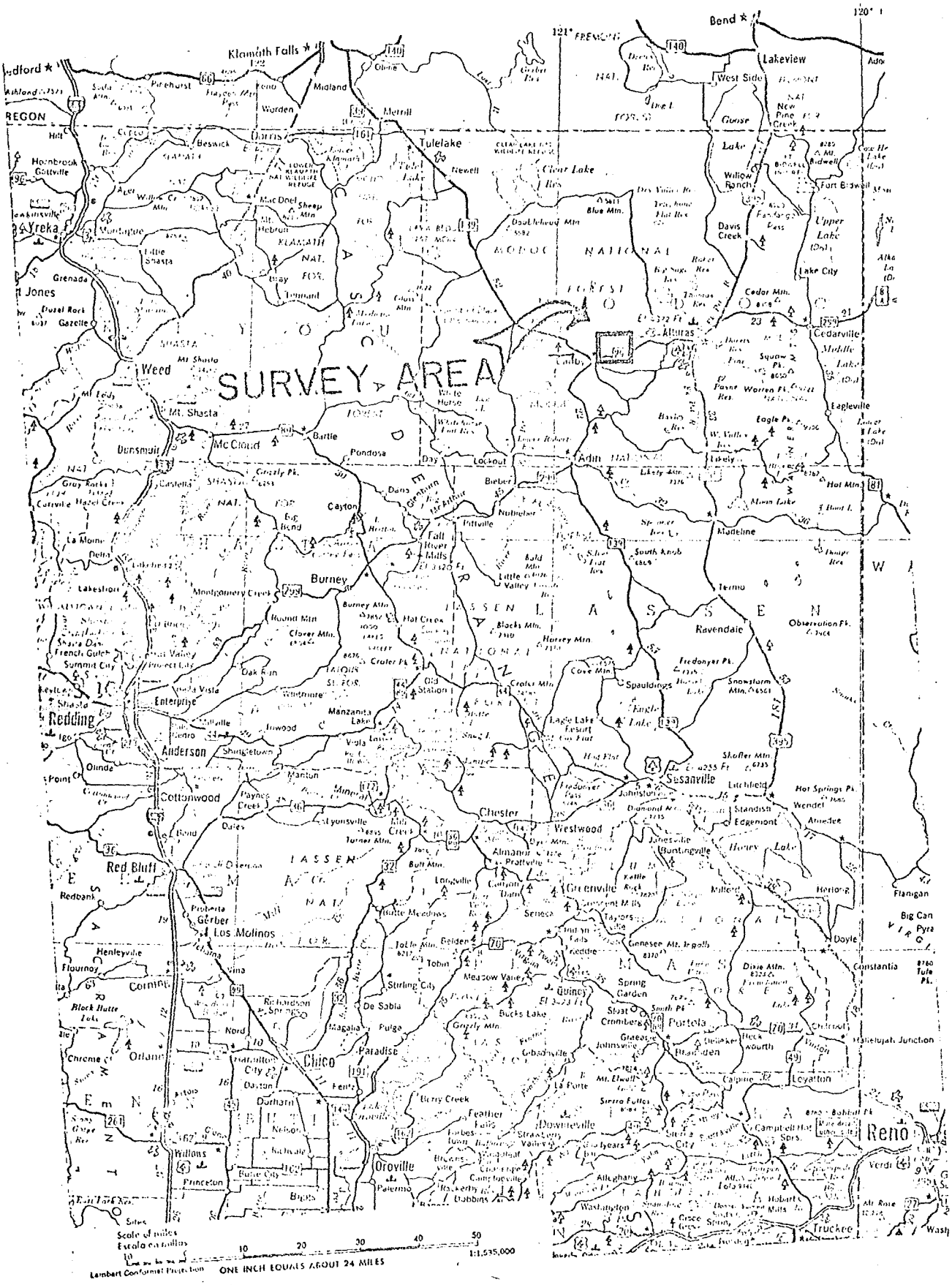

Figure 1: Road map of northeastern California showing location of Kelly Hot Spring electrical geophysical survey.

Tertiary and Quaternary deposits, both fluvial and lacustrine. Diatomaceous sandstones and shales, tuff beds, and tuffaceous sandstones are also common.

The volcanic rocks and associated continental deposits reach great thicknesses as evidenced by the outcrop section of more than 5000 feet exposed in the Warner Range (MacDonald, 1966) to the east of the survey area, and by wells drilled by the Humble Oil and Refining Company in southern Oregon (Chapman and Bishop, 1968). The Thomas Creek unit well #1 in sec. 18, T. 36 S., R. 18 E., located on a structural high about 30 miles north of the California border, was still drilling in volcanic and continental deposits at its total depth of 12,093 feet.

Because most of the Modoc Plateau is covered by the Tertairy and Quaternary volcanic deposits mentioned above, little is known of the regional geologic structure in the underlying rocks. At present gravity is the only regional geophysical information available for studying these hidden structures on a regional scale (see Chapman and Bishop (1968) from which this section was abstracted).

According to LaFehr (1965) the regional gravity field in northeastern California decreases from about -120 mgal. in the southwest (about 41°North, 122°West) to less than -160 mgal. in the northeast (about 42°North, 120°West). This decrease is probably related to an eastward thickening of the continental crust.

Some of the local gravity anomalies of the the Modoc Plateau are associated with exposures of particular rock types, such as pre-Tertiary basement rocks, Tertiary intrusives, and Quaternary sediments. A number of other local anomalies located within the areas covered by Tertiary and Quaternary volcanic rocks show no obvious relation to rock type. These anomalies (all positive) reach amplitudes as great as 20 mgal. and are found southeast of Tule Lake, northwest of Adin, north-

west of Klamath Lake, and both northeast and west of Alturas. Possible causes include near-surface basement rocks, near-surface intrusive rocks, or lateral density changes within the volcanic rocks. Several of these positive anomalies are located along a northeast-trending line between points northwest of Adin and east of Goose Lake. The direction of this possible trend is nearly 90° to the direction of basin and range structure shown in the Warner Range.

One of the most prominent faults in the Modoc Plateau is the Likely Fault which extends from a point northwest of Canby southeastward to near Madeline and which is believed to be a major strike slip fault (Gay, 1959). The gravity field is not noticeably influenced by the fault, although the data are rather sparse in much of this area.

The part of the gravity map by Chapman and Bishop (1968) which covers the survey area is shown in Figure 2. Its relationship to the electrical survey will be discussed later.

Plan of the Electrical Survey

The electrical resistivity of a rock is a measure of the resistance to the flow of electrical current and is determined almost entirely by the amount and resistivity of the water contained in its pores. The water resistivity depends on the nature of the dissolved salts and on temperature. It is this dependence on temperature that makes electrical resistivity measurements such a useful technique in investigating geothermal systems. With an increase in temperature and in the amount of dissolved salts, the resistivity of a rock will decrease until the boiling point is reached, past which the resistivity rapidly increases. The ratio of the resistivity of the host rock to that in the geothermal cell is defined as the Geothermal Resistivity Index (GRI). If the salinity of the pore water is the same in the geothermal reservoir and in the host rock, then the GRI is a very good indication

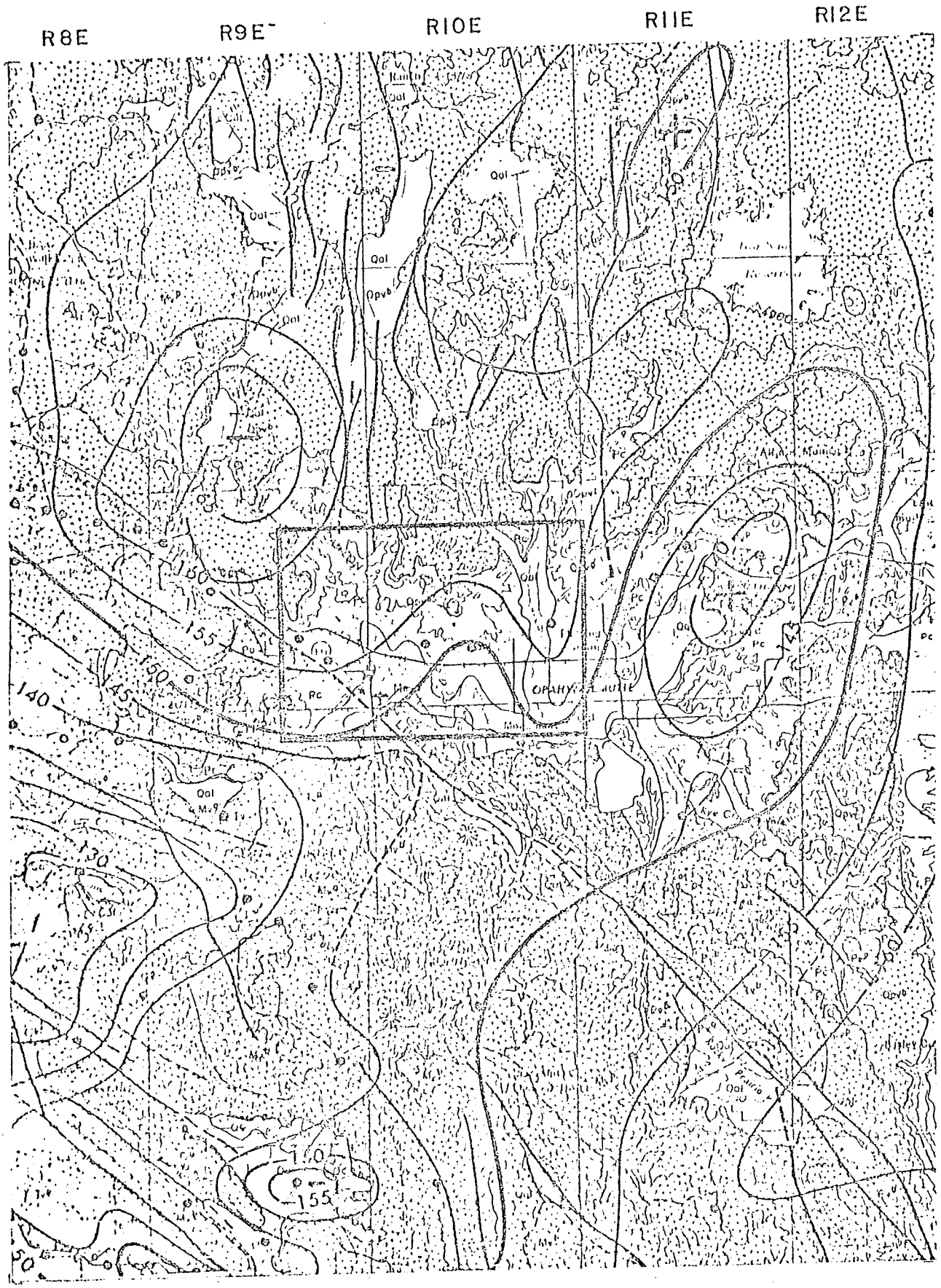

Figure 2: Regional gravity map (from Chapman and Bishop, 1968). Rectangle shows area covered by Figures 4,5,6.

of the elevation of temperature inside the cell and must be at least 5 if the reservoir is to produce power (Dr. George Keller, Colorado School of Mines, personal communication). In surveys conducted in other geothermal areas, dipole mapping surveys (also called controlled-source telluric-current technique (Furgerson, 1970), total-field resistivity mapping (Zohdy, 1973), roving dipole, and dipole-dipole mapping) have been found to be an efficient means for locating the low resistivity regions about geothermal cells.

Dipole mapping surveys are useful in mapping the geographical extent of deep-lying geothermal reservoirs, but provide only a minimum amount of information on the variation of resistivity with depth in the ground. Once the extent of a reservoir has been determined, other electrical methods are usually used to determine the depth to the top and bottom of the reservoir. Such information can be obtained with Schlumberger soundings and/or the electromagnetic sounding method after dipole mapping is completed.

Dipole Mapping Survey

In a dipole mapping survey (Furgerson, 1970, 1973), a large amount of electric current is caused to flow in the earth between electrode contacts situated within a few miles of the target area. As the current flows through the ground from this "dipole" source, its flow pattern will be governed by variations in resistivity in the ground to a depth comparable to the offset distance at which the measurements are being made. Because the dipole source is fixed in location while many measurements of electric field are made about it, any electrical non-uniformities near the source will affect all the measurements similarly, and the variation in the characteristics of the electric field from observation point to observation point will be indicative of the electrical

structure of the ground primarily in the vicinity of the measurement points.

The general scheme of a dipole mapping survey is indicated in Figure 3. A and B are current electrodes, MN_1 and MN_2 are voltage measuring dipoles, δ is the angle between the measuring point and the source electrodes, θ is the angle between the voltage measuring dipoles, and R_1 and R_2 are the distances from the measuring point to the source electrodes. This array is superficially similar to an azimuthal dipole-dipole array. However, for the electrode separations $\overline{AB}$ and $\overline{MN}$ to approximate true dipoles, the separation between them should be at least five times greater than the larger of $\overline{AB}$ or $\overline{MN}$ (Alpin, 1966). Experience, however, shows that for a large $\overline{AB}$, practical current moments of 2000 to 200,000 ampmeters give reliable field strengths for distances up to five or at the most ten times $\overline{AB}$. The parameter "current moment" is defined as the product of the current flowing into the ground through the current electrodes times the distance between the current electrodes. For a given resistivity distribution in the ground, the field strength at a particular observation point is proportional to the current moment. Thus most of the stations must be located at distances R_1 for which the array is more properly termed a quadripole array for a very small R_1 or a pole-bipole array for a larger R_1.

A source dipole 1.3 miles long was used in this survey, and the source electrodes were grounded through road culverts. Power was provided to the source dipole from a 30 KW motor-generator set. The 208-volt 60-Hz three-phase output of the generator was stepped up to 440 volts with a transformer, rectified to form direct current, and alternately switched to cause current to flow first one way and then the other in the line connecting the source electrodes. The period between one complete cycle of current flow was selected to be 20 seconds, so that the frequencies contained in the waveform would be sufficiently low to avoid problems with electro-

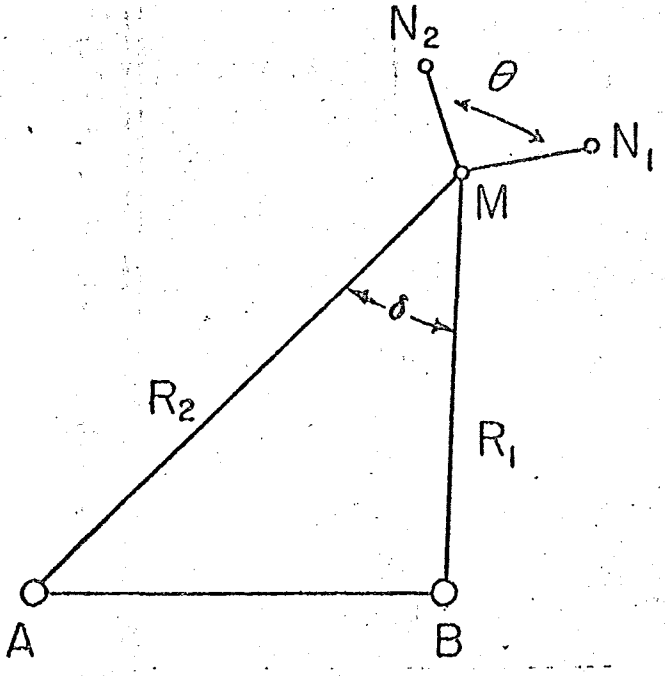

Figure 3: General scheme of a dipole mapping survey.

magnetic attenuation of the current field and lack of penetration caused by skin-depth effects. The current waveform was asymmetrical to provide a means for assigning a polarity to voltage detected at the receiving sites. The amplitude of the current steps was recorded graphically, and current steps with amplitudes of 23 to 28 amperes were obtained.

The electric field from a source dipole was mapped by measuring voltages between electrode pairs at many points about the source dipole. Because the direction of current flow at a measurement site is quite unpredictable, the total voltage drop must be determined by making measurements with two electrode pairs oriented at close to right angles to one another and adding voltages vectorially. The electric field is then assumed to be the ratio of voltage drop to the separation between the measuring electrodes. Measurements were made with receiving electrode separations of 300 feet. The receiver was a sensitive DC voltmeter and consisted of a high-gain, low-noise, operational amplifier with high input impedence (1×10^6 ohms), coarse and fine DC offsets, and a maximum sensitivity of 20 microvolts per dial division. An output jack enabled chart recording of the data when desired.

Electric fields were measured at distances from the source dipole ranging up to $3\frac{1}{2}$ miles (see Figure 4 for station location map). Measurements were not made closer than about one-half mile from the end of the source dipole, because an advantage in using the dipole mapping technique lies in the capacity to make measurements at sufficient distance to assure penetration to depths of many thousands of feet. Measurements made close to one end of a dipole source will reflect the resistivity only to a shallow depth, comparable to the distance from the end of the line. The primary data obtained are listed in Appendix A. These data may be converted to apparent resistivity values using several different formulas.

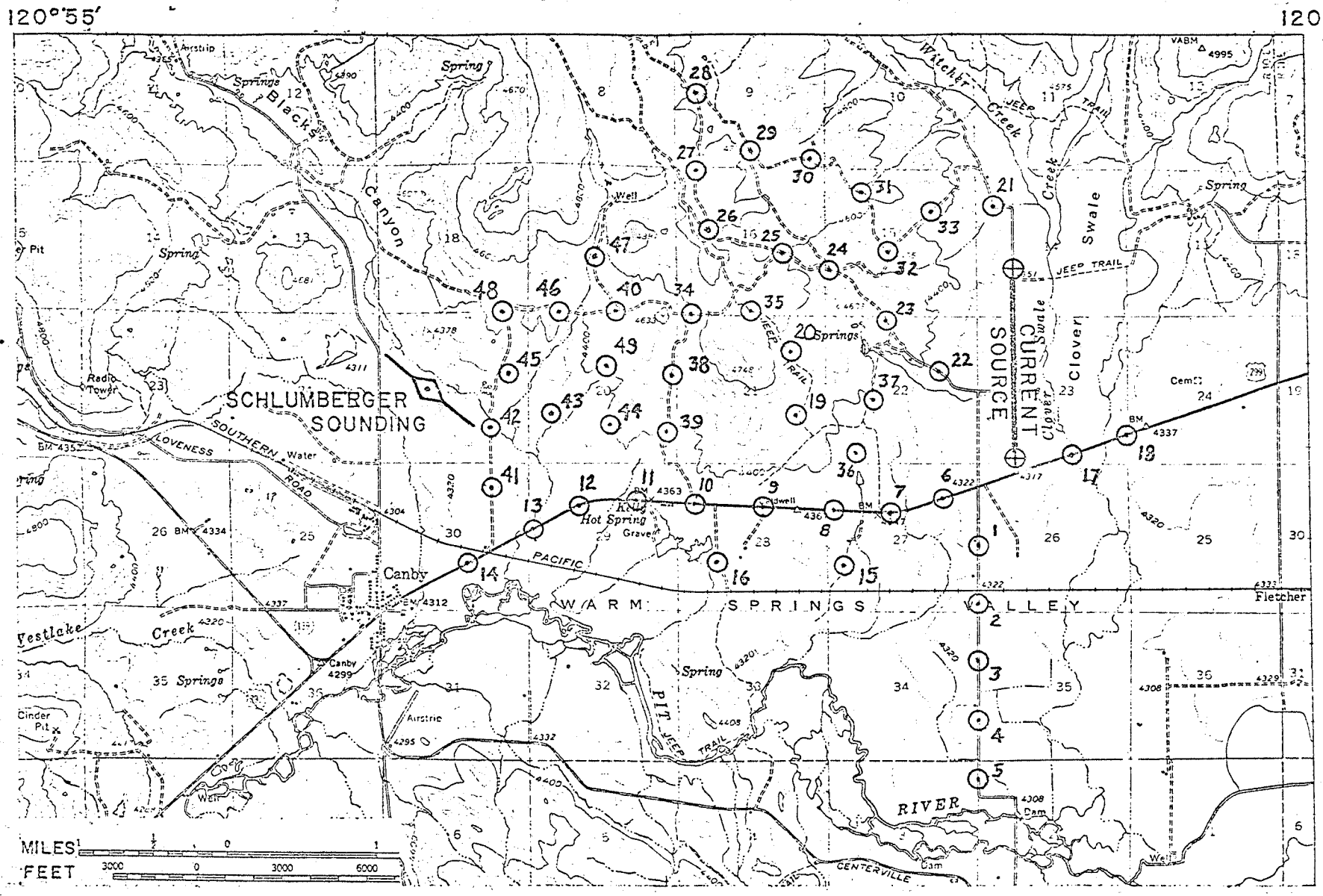

Figure 4: Locations of Schlumberger sounding and dipole mapping source and receiver stations.

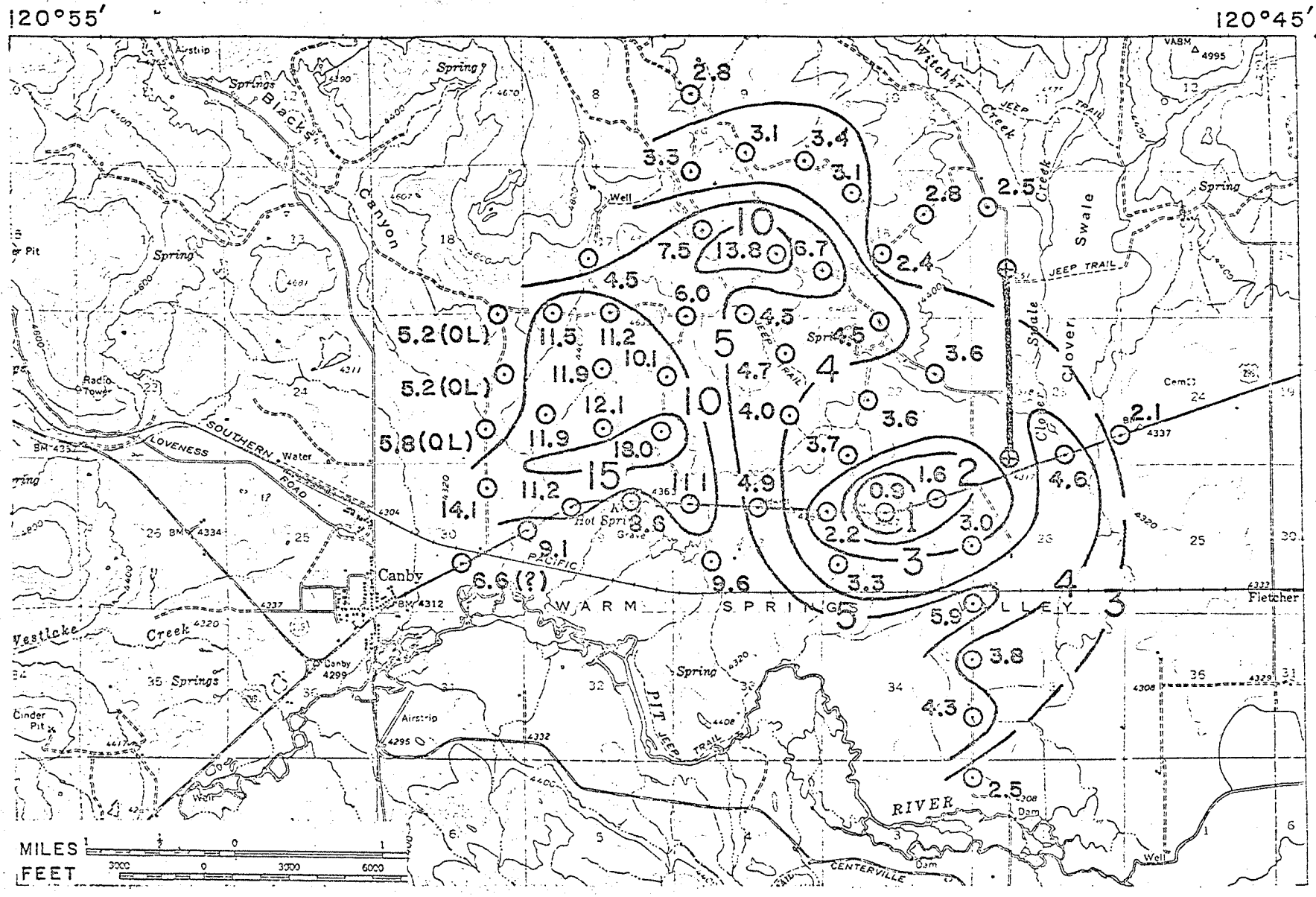

Figure 5: Apparent resistivity in ohm-meters; (OL) = or less

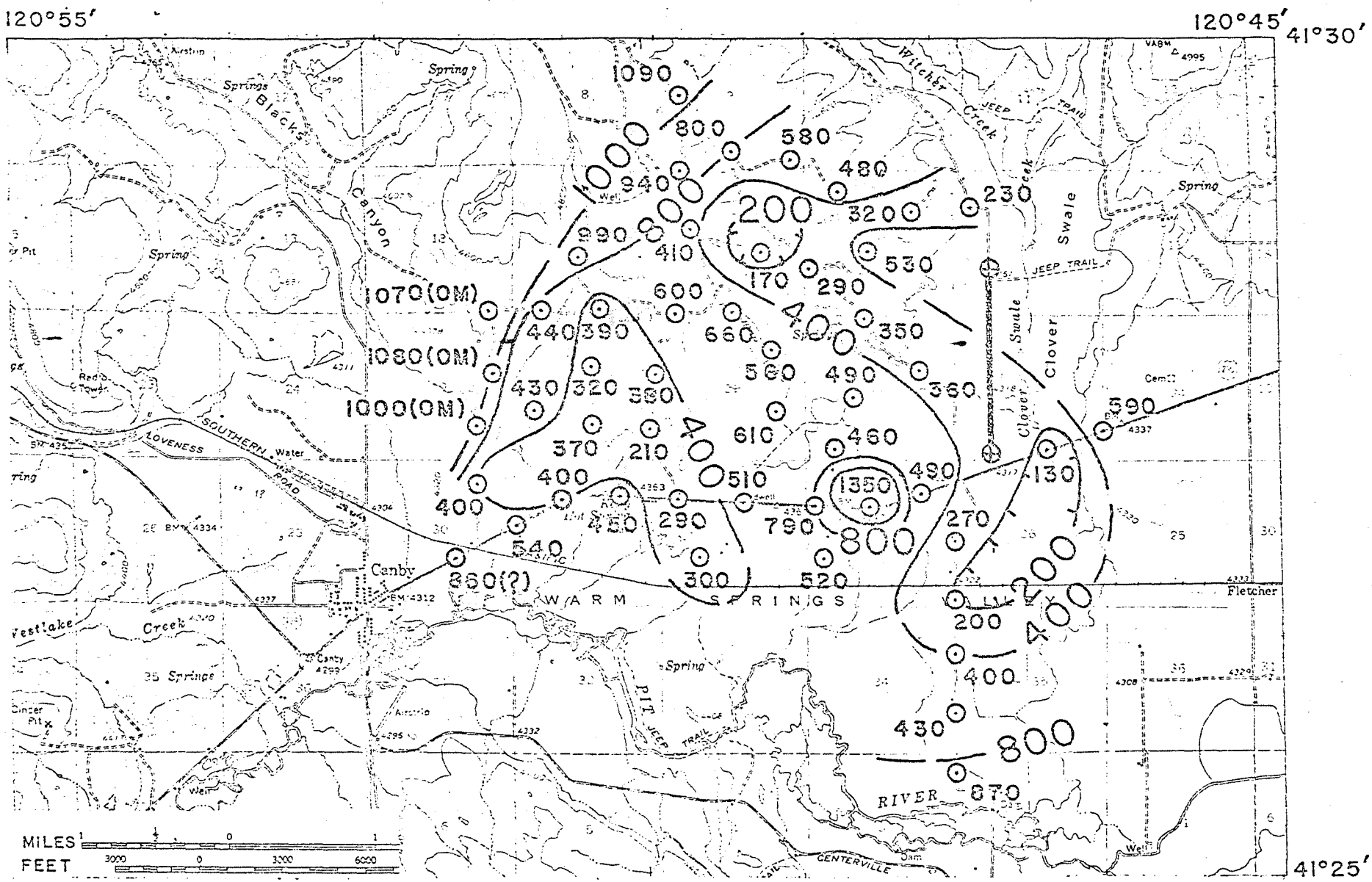

Figure 6: Apparent conductance in mhos; (OM) = or more.

The conventional manner of defining apparent resistivity is to consider what resistivity a uniform earth would require to provide the voltages actually measured. In a uniform earth, current spreads out from a single electrode with spherical symmetry. The electric field strength on the surface of the earth at a distance R_1 from a single electrode through which a current I is passing is then

$$E_1 = \frac{\rho I}{2\pi R_1^2}$$

where ρ is the resistivity of the assumed uniform earth. When a dipole pair of electrodes is used for a current source, there is a second contribution to the electric field from current flowing through the second electrode:

$$E_2 = \frac{\rho I}{2\pi R_2^2}$$

where R_2 is the distance from the observation point to the second current electrode. The electric fields E_1 and E_2 are vector quantities and must be added vectorially. The vector sum is

$$E_T = \frac{\rho I}{2\pi R_1^2}\left[1 + \left(\frac{R_1}{R_2}\right)^4 - 2\left(\frac{R_1}{R_2}\right)^2 \cos\delta\right]^{1/2}$$

Solving this expression for ρ provides the means for computing apparent resistivity under the assumption of spherically-symmetric spreading of current in a uniform earth. Values for apparent resistivity computed with this formula are listed in Appendix A. These same data were used to compile the contour map shown in Figure 5.

A second common model is one where conductive rocks overlay a highly resistant substratum, such as crystalline basement rocks. For this layered model, the apparent resistivity increases linearly with distance from the source dipole for

distances greater than the depth to the resistant rock. Since the current is constrained to flow almost entirely in the surface layer of conductive rock, the calculation of resistivity on the basis of an assumed spherical spreading of the current seems inappropriate. In this case, a more meaningful way to reduce the field data might be to use a formula based on the assumption of cylindrical spreading. For current spreading through a plate, the electric field depends on the ratio of plate thickness (h) to resistivity (ρ), h/ρ, a quantity which is also known as the conductance of the plate, S. The electric field at the surface of the plate for a current I to a single electrode is

$$E_1 = \frac{I}{2\pi S R_1}$$

where R_1 again is the distance from the first current electrode to the observation point. With the addition of a second electrode to complete the dipole current source, the contribution of a second electric field at the observation point must be considered

$$E_2 = \frac{-I}{2\pi S R_2}$$

The vector sum of these two electric fields is

$$E_T = \frac{I}{2\pi S R_1}\left[1 + \left(\frac{R_1}{R_2}\right)^2 - 2\left(\frac{R_1}{R_2}\right)\cos\delta\right]^{1/2}$$

Solving this expression for S provides the means for computing apparent conductance under the assumption of cylindrically-symmetric spreading of current in a uniform conducting plate. Values for apparent conductance computed with this formula are also listed in Appendix A. These same data were used to compile the contour map shown in Figure 6.

Schlumberger Sounding

An electrical resistivity sounding consists of a succession of apparent resistivity measurements made with an increasing electrode separation, the center of the configuration and its orientation remaining constant. With larger electrode separations, the effect of material at depth becomes more pronounced, and thus the apparent resistivity values made at the ground surface reflect the vertical distribution of resistivity values in a geological section. There are rather severe limits on the amount of lateral variation in resistivity permitted with this method.

The Schlumberger electrode configuration (Chastenet de Gery and Kunetz, 1956; Keller and Frischknecht, 1966) consists of two current electrodes, A and B, and two potential electrodes, M and N, spaced along a straight line as shown in Figure 7. The potential electrodes are placed an equal distance about the midpoint between the current electrodes and are kept sufficiently close together so that the electric field between them can be considered constant. In practice, the separation of potential electrodes M and N is always kept less than one-fifth of the separation between the current electrodes A and B. The formula used for the apparent resistivity is

$$\rho_a = K \frac{\Delta V}{I}$$

where ΔV is the potential difference between the potential electrodes, I is the current input to the ground between the current electrodes, and K is the geometric factor which takes the exact location of all four of the electrodes into account

$$K = \frac{2\pi}{\frac{1}{AM} - \frac{1}{AN} - \frac{1}{BM} + \frac{1}{BN}}$$

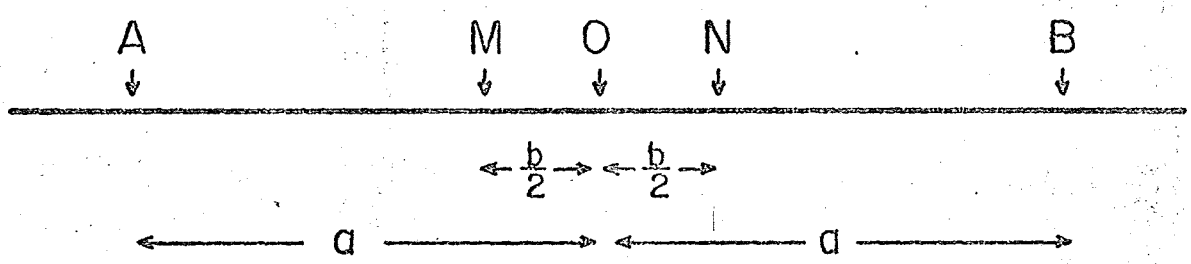

Figure 7: Schlumberger electrode array geometry.

With the symmetry described above and letting AB/2 = a and MN = b

$$K = \pi\left(\frac{a^2}{b} - \frac{b}{4}\right)$$

Only one set of electrodes, either the current or the potential, is moved between successive measurements. Thus the potential electrodes remain fixed for several (usually 3 to 5) increasingly expanded current electrode spacings. The location of the sounding center and the direction of electrode expansion are shown on Figure 4. Measurements were made with "a" spacings of 20 feet minimum to 3000 feet maximum and were spaced to give about 7 points per decade on a logarithmic plot of AB/2 versus apparent resistivity. The field data are represented by points enclosed in circles on Figure 8.

The transmitter and receiver were the same as that used in the dipole mapping survey. The output waveform is a square wave, and the frequency and wave symmetry are variable. The frequencies used in the sounding varied between 0.2 and 0.0125 Hz and generally were selected by consideration of the skin depth, the depth at which the amplitude of an electromagnetic wave is reduced to 1/e of its surface value (Stacy, 1969). When the frequency is too high for the depth-resistivity combination, the apparent resistivity obtained will be too high. A simple empirical test (Meidav and Furgerson, 1972) was used to determine the reliability of a measurement. Readings were taken at more than one frequency at a given electrode spacing. Hence, a difference in potential electrode voltage of more than 3 to 5 percent between two frequencies was used to judge the quality of the data. The data obtained with longer periods were deemed more reliable. Coupling between current and potential lines and grounded fences caused extreme problems during the first day of Schlumberger sounding, but

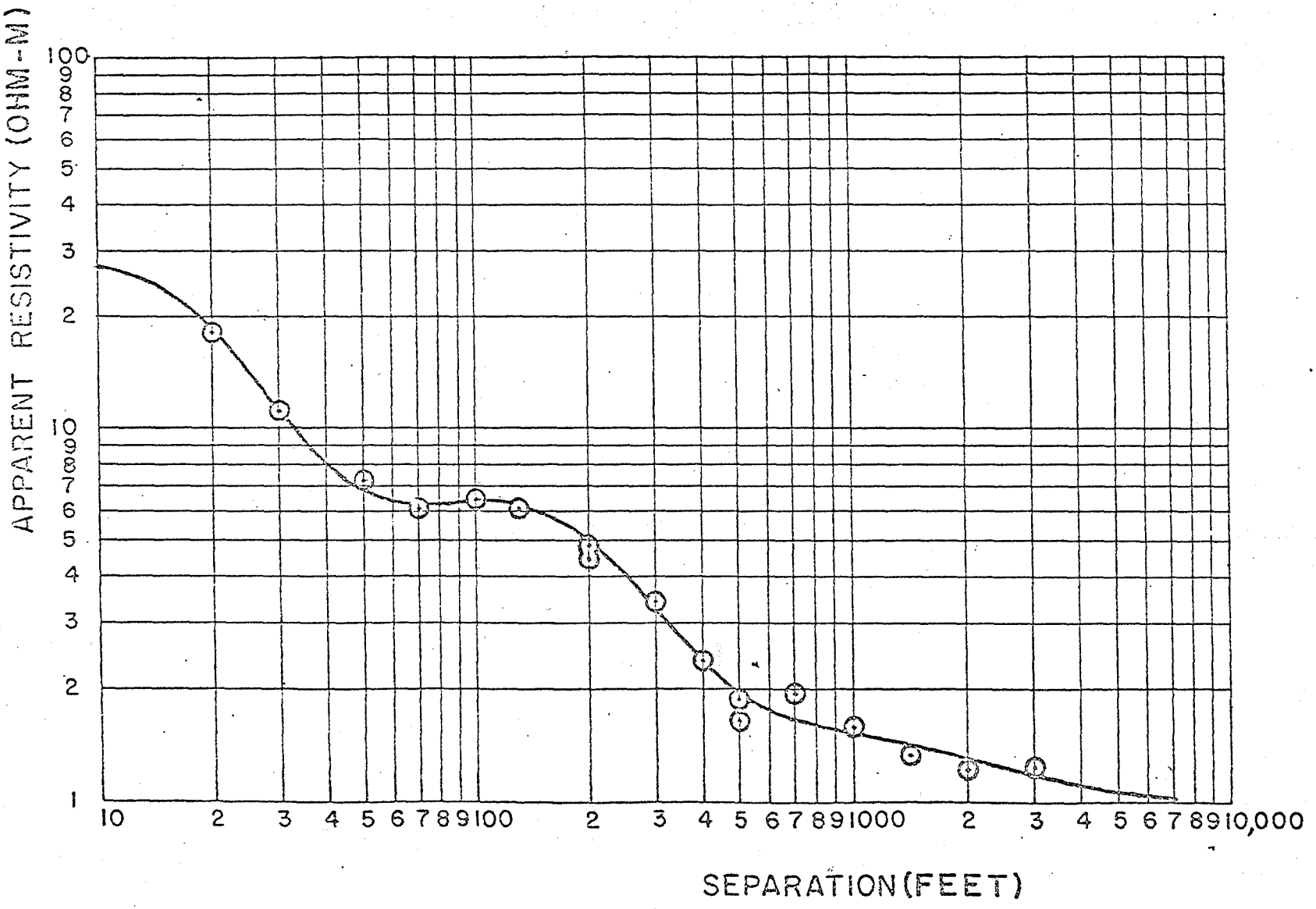

Figure 8: Schlumberger sounding field data (points in circles) and interpretation (solid line).

it was greatly reduced the second day by keeping the wires at least 1000 feet from the grounded fecnes and /or crossing the grounded fences at 45^{o} or more.

Interpretation consisted of decomposing (or inverting) the field curve into layer thicknesses and layer resistivities, assuming a horizontally-layered structure. How "true" the values of thickness and resistivity are depends on the degree of validity of assuming a horizontally-layered structure; how equivalent the curve is; the available correlations; and the technique used in accomplishing the actual inversion. Decomposition consisted of three steps. The first involved making a graphical interpretation by the auxiliary point method (Zohdy, 1965; and Orellana and Mooney, 1966). In the second the auxiliary interpretation and the field curve were input into a computer program developed by Crous (1971) which Hankel-transforms the field data into the "kernal" domain and, with the auxiliary curve interpretation as a first cut, arrives at an interpretation by a least squares fitting routine. The output is in terms of each layer's longitudinal conductance (S) or transverse resistance (T). In the third step the values of S and T were input into a computer program which computes theoretical sounding curves for the Schlumberger array over a multi-layered horizontal earth (Argelo, 1967). The theoretical curve obtained by the above procedure is represented by the solid line on Figure 8.

Evaluation of the Survey Data

It must be stressed that the apparent values for resistivity or conductance calculated from dipole mapping data are the actual values only in the case in which the structure of the earth is as simple as that assumed in defining these quantities. That is, the earth must be completely uniform laterally. However, if a conductive geothermal reservoir is present in the survey area, we expect this condition to be violated. The

computed values of apparent resistivity and apparent conductance will be functions of any lateral changes in resistivity which are present.

The calculation of apparent resistivity is based on the model of a completely uniform earth. In many survey areas, in addition to the anomalous conductivity associated with a geothermal cell, there is a marked contrast in resistivity between the porous section in which the geothermal reservoir exists and the underlying basement. For measurements made at distances from the source greater than the depth to basement, the apparent resistivity value computed from the field measurements mainly reflects the higher basement resistivity. When this effect is present, apparent resistivity contours form an elliptical pattern about the source (see theoretical map of Figure 9). The eccentricity of the ellipses reflects the well-known fact that measurements made along the polar axis of a dipole source do not detect the presence of a resistant basement until larger spacings are reached than are required when measurements are made along the equatorial axis (Keller and Frischknecht, 1966). It should also be noted that there are two small regions about the ends of the dipole where the apparent resistivity is lower than unity, the resistivity assigned to the surface layer. The elliptic behavior makes it more difficult to see the patterns in resistivity which may be associated with local anomalies such as are present in geothermal cells, and in addition, makes it difficult to superimpose measurements made from different dipole sources on a common map.

This problem for the layered model can be eliminated to a considerable degree by using the apparent conductance values, computed on the assumption that current spreads through a conducting plate. The thickness of the plate (that is, the thickness of the porous part of the section) need not be known, if the distance at which measurements are made is greater than

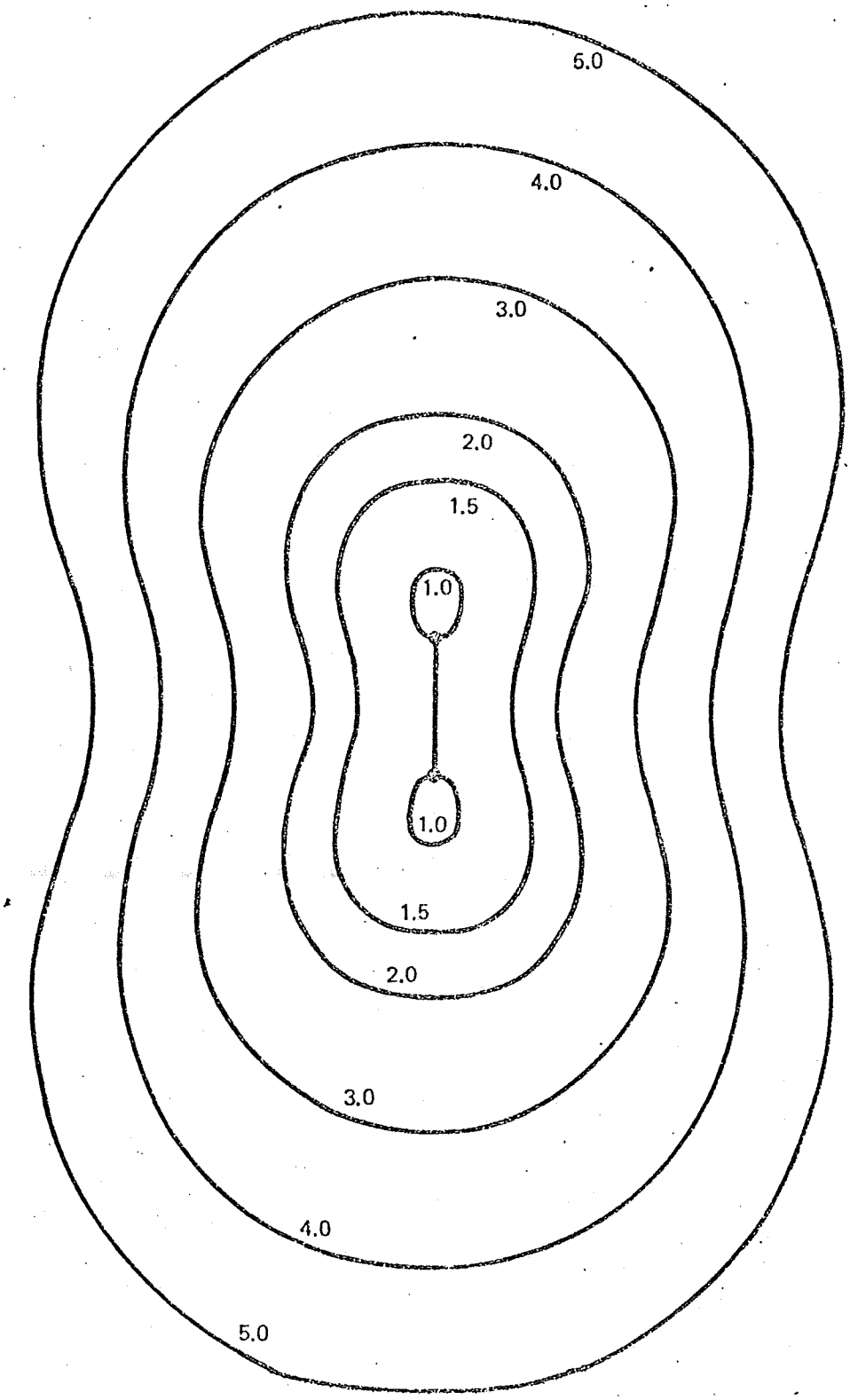

Figure 9 : Apparent resistivity dipole map for the case of a two layer sequence in which the surface layer has unit resistivity, the second layer resistivity is 1000 times that of the first layer, and the thickness of the first layer is half of the source dipole length.(from Furgerson and Keller, 1973).

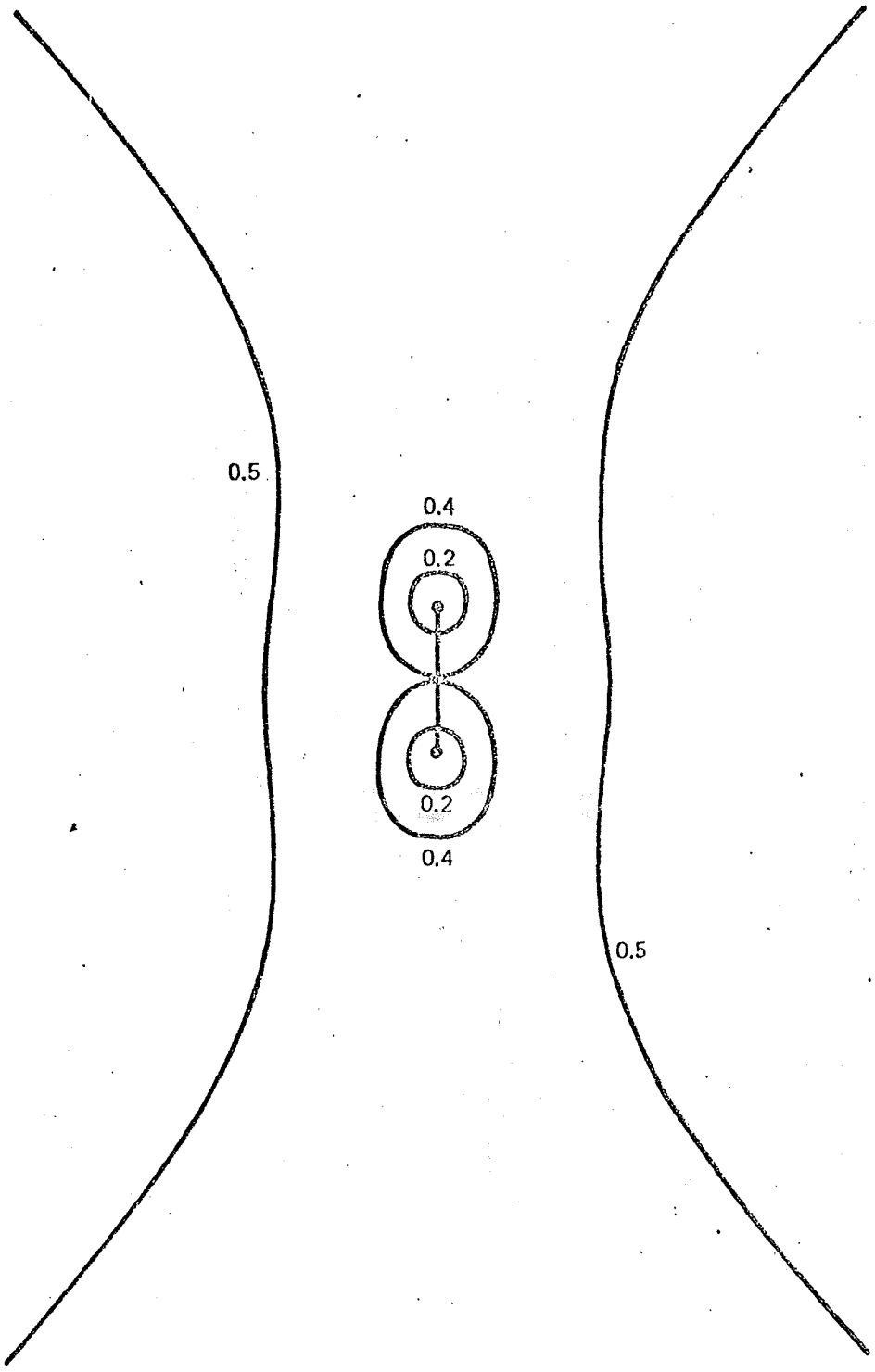

Figure 10: Apparent conductance dipole map for the case of a two layer sequence in which the surface layer has unit resistivity, the second layer resistivity is 1000 times that of the first layer, and the thickness of the first layer is half of the source dipole length (from Furgerson and Keller, 1973).

the plate thickness. In contrast to the large variations in apparent resistivity as a function of distance from the source, the values of apparent conductance show very little change over most of the theoretical map (Figure 10), after reaching some 98 percent of the correct value of conductance for the surface layer at a distance of about one unit from the dipole. The shape of the contours several source lengths away from the source are roughly hyperbolic.

The relative merits of apparent resistivity and apparent conductance may be investigated in several ways. One of these is to consider the distribution patterns for the two quantities (Figure 11). These distributions are histograms for the frequency of occurrence of measured values (as tabulated in Appendix A and contoured in Figures 5 and 6), with the intervals over which the histograms are compiled being taken as geometric progressions. Both histograms appear to be bimodal with apparent-resistivity medians of 3.1 and 12.1 ohm-meters and with apparent-conductance medians of 480 and 970 mhos. The bimodal character is typical of theoretically computed maps in which the electrical properties vary laterally (Furgerson and Keller, 1973).

With the bimodal character as background, an analysis of the electrical structure can be made. The higher apparent-conductance median of 970 mhos is produced by two areas on Figure 6. One of these is a closed, circular anomaly in the north half of section 27, T.42N.,R.10E., and the second is the area west of a reasonably straight line running N.30°E. through sections 19, 11, and 9, T.42N.,R.10E. The rest of the mapped area conforms reasonable well to the other apparent-conductance median of 480 mhos. This is especially true when it is observed that the apparent-conductance histogram (Figure 11) shows marked skewing towards lower values from the 480 mho median.

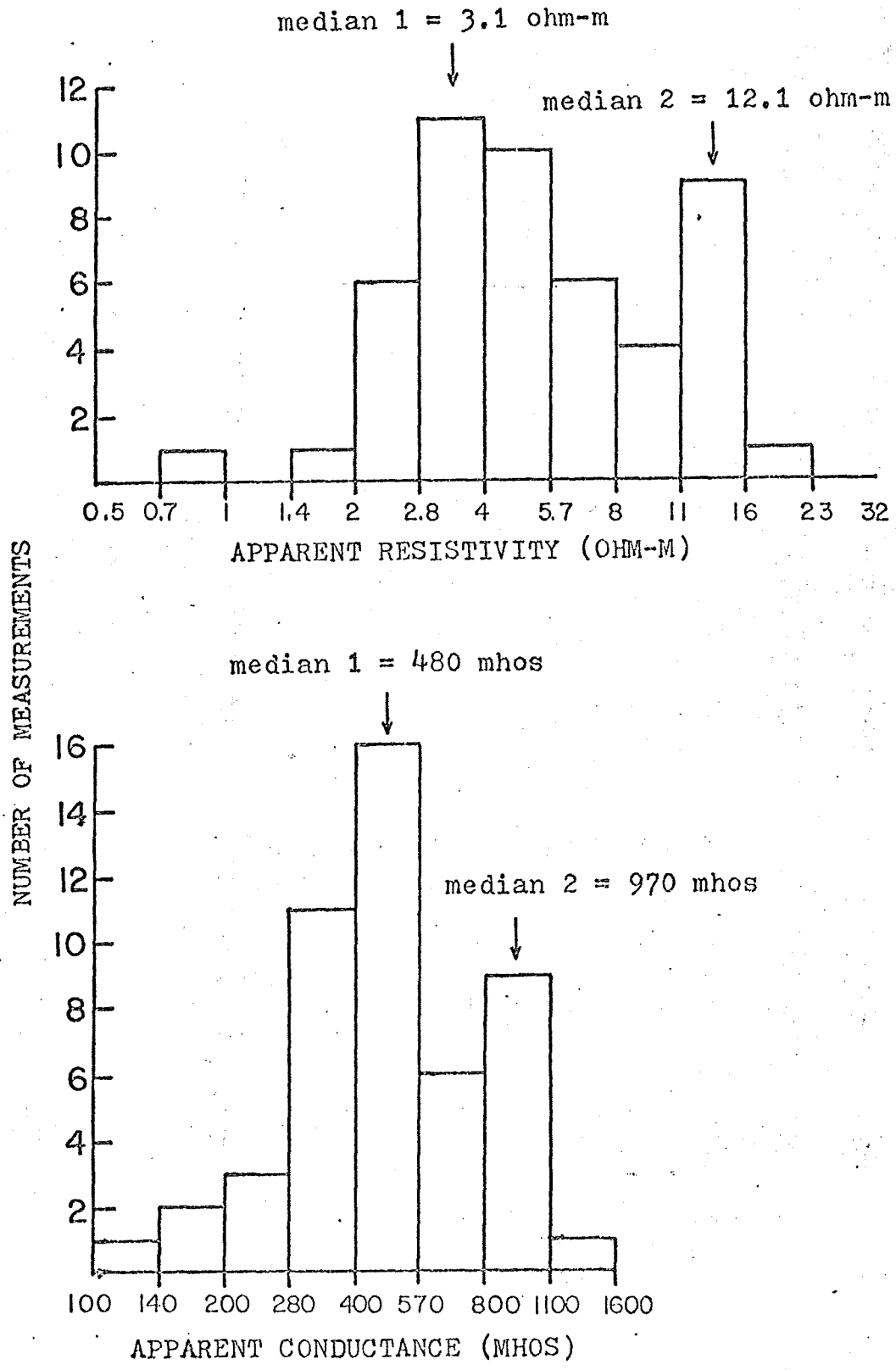

Figure 11: Histograms showing the distribution of dipole mapping values for apparent resistivity and apparent conductance.

The N.30°E. boundary was theoretically modeled as a steeply dipping contact between two media of differing electrical properties, both of which lie on a basement of high resistivity. This was done because the apparent conductance measured in the region on the far side of the contact from a source dipole will be less than the true conductance. The study showed that the true conductance to the west of the N.30°E. boundary is probably closer to 1700 mhos. In fact, because signal levels to the west of the N.30°E. boundary were very low as a result of the high conductance and large distance from the source, the apparent conductance values obtained are probably to low and, therefore, the true conductance may be even higher than 1700 mhos.

As might be expected in an area of complex electrical structure, the apparent-resistivity medians do not appear to correspond to the same map regions as the apparent-conductance medians. The higher apparent-resistivity median of 12.1 ohm-meters corresponds to a dike-like band of high resistivities trending N.30°E. and bounded on the northwest by the N.30°E. conductance boundary discussed previously and on the southeast by a much more poorly defined line trending N.30°E. through sections 29, 21, and 15, T.42N., R.10E. Looking carefully again at the apparent-conductance map and histogram, the same dike-like trend can be roughly seen in the 200 to 300 mho lows in the SW corner of sec. 20 and the east half of sec. 16, T.42N., R.10E. Both the apparent-resistivity and apparent-conductance dike-like trends appear to be broken by a northwest trend through the SW corner of sec. 16, T.42N. R.10E. Both are truncated on the northeast at about the NE corner of sec. 16, T.42N., R.10E., and may by truncated on the southwest although data is sparse in this area. The second apparent-resistivity median of 3.1 ohm-meters corresponds to the area southeast and northeast of the dike-like trend and outside the very low resistivity, closed, circular anomaly in the northern half of sec. 27, T.42N., R.10E.

The resistivities of the stations (42, 45, and 48 on Figure 4) northwest of the N.30°E. line marking the boundary of the inferred 1700 mho or greater conductance region are only maximum values because of the low signal level. In order to more accurately confirm the resistivity of this very promising region, a Schlumberger sounding was made in the west half of sec. 19, T.42N., R.10E. (see Figure 4 for location and Figure 8 for data). The sounding was made at the end of the survey and unfortunately could not be continued past 3000 feet AB/2, because a weather front moved in with rain, hail, and 40 m.p.h. winds. The interpretation procedure outlined earlier gave the following results:

resistivity in ohm-meters	depth extent in feet
30	0 to 11
4.4	11 to 44
50	44 to 55
1.5	55 to 1000
1.0	1000 to 3000 or more

This is very encouraging. If we use the conductance value of 1700 mhos derived earlier and the above sounding information, a 5000 ft thick section of low resistivity material appears to be indicated.

The circular anomaly in sec. 27, T.42N., R.10E. is also a very promising anomaly, and its map extent is delineated by the 800 mho contour of Figure 6. Good depth extent is suggested by its 0.65 to 1.25 mile distance from the nearest current electrode. Such a distance from the current source virtually eliminates the possibility that the anomaly is a surface feature.

The gravity map discussed earlier on a regional basis tends to support the electrical interpretations and suggests one possibility for the heat source. The electrical survey

area is outlined on the gravity map in Figure 2, and although the gravity data is sparse shows some very interesting features. A local gravity high separating two lows is indicated by the -155 and -150 mgal. contours. The high is situated a little east of and trends in the same direction as the dike-like band of high resistivity, and may represent a near surface intrusive and be the heat source for the geothermal features observed at the surface. The two flanking lows suggest lower density, higher porosity material and probably corresponds, at least in part, to the two highly conductive anomalies.

Conclusions and Recommendations

The results of the electrical geophysical survey should be integrated with the results of other geological and geophysical surveys carried out in the area to assure that the interpretations presented here are compatable with all the information available. Presuming they are, the electrical geophysical survey points to two locations as being the most likely for testing of the geothermal power production capacity of the prospect. The first is a closed, circular anomaly in the northern half of sec. 27, T.42N., R.10E. and is delineated by the 800 mho contour on Figure 6. The second is the area northwest of a line trending about N.30°E. through sections 19, 11, and 9, T.42N.,R.10E. and is delineated by the 1000 mho contour on Figure 6. The data also suggest that holes must be drilled to depths of 2000 feet or more to test the low-resistivity porous interval where geothermal production would be expected to be obtained.

The first of the above anomalies (sec. 27, T.42N., R.10E.) is suggested as the one to test first. The most obvious reason is that it is the only one located on land already leased. The second reason is that the western anomaly, although highly promising , has been delineated only on one side. Experience

in other geothermal areas shows that most economic geothermal cells are characterized by closed electrical anomalies. The western anomaly may indeed close to the west, but more electrical work is recommended before deciding to locate a test.

It is therefore recommended that a leasing program be initiated to acquire additional land south to the tracks of the Southern Pacific Railroad and west to at least the road running north-south through Canby. A dipole source should be situated somewhere north of Canby to test the western area. One or more electrical soundings in the western anomaly would also be recommended, as well as one in the eastern anomaly (sec. 27, T.42N., R.10E.).

References

Alpin, L. M., 1966, The theory of dipole sounding in Dipole methods for measuring earth conductivity: New York, Consultant's Bureau, 302 p.

Argelo, S. M., 1967, Two computer programs for the calculation of standard graphs for resistivity prospecting: Geophysical Prospecting, v. 15, no. 1, pp. 71-92.

Chapman, R. H., and Bishop, C. C., 1968, Bouguer gravity map of California (Alturas sheer); California Division of Mines and Geology.

Chastenet de Gery, Jerome, and Kunetz, Geza, 1956, Potential and apparent resistivity over dipping beds: Geophysics, v. 21, pp. 780-793.

Crous, C. M., 1971, Computer-assisted interpretation of electrical soundings: M.Sc. thesis, Colorado School of Mines.

Furgerson, Robert B., 1970, A controlled-source telluric current technique and its application to structural investigations: M.Sc. thesis, Colorado School of Mines.

_____, 1973, Progress report on electrical resistivity studies, Coso Geothermal area, Inyo County, California: TP 5497, Naval Weapons Center, China Lake, California, UNCLASSIFIED--APPROVED FOR PUBLIC RELEASE.

_____ and Keller, George, 1973, Catalogue of dipole mapping curves and profiles: Office of Naval Research report, in preparation.

Gay, T. E., 1959, Geology of northeastern California: California Div. Mines and Geology, Mineral Information Service, v. 12, no. 6, p. 1-7.

Keller, G. V., and Frischknecht, F. C., 1966, Electrical methods in geophysical prospecting: New York, Pergamon Press.

La Fehr, T. R., 1965, Gravity, isostasy, and crustal structure

in the southern Cascade Range: Jour. Geophys, Research, v. 70, p. 5581-5597.

MacDonald, G. A., 1966, Geology of the Cascade Range and Modoc Plateau in Bailey, E. H., ed., Geology of northern California: California Div. Mines and Geology, Bull. 190, p. 65-96.

Meidav, Tsvi, and Furgerson, R. B., 1972, Resistivity studies of the Imperial Valley Geothermal area, California: Geothermics, v. 1, no. 2, p. 46-62.

Orellana, E., and Mooney, H.M., 1966, Master tables and curves for vertical electrical sounding over layered structures: Madrid, Interciencia.

Stacey, F.D., 1969, Phusics of the earth: New York, Wiley, 324 p.

Stanley, W. D., and others, 1973, Preliminary results of geophysical investigations near Clear Lake, California: U.S.G.S. open-file map.

Zohdy, Adel, 1965, The auxiliary point method of electrical sounding and its relationship to the Dar Zarrouk parameters: Geophysics, v. 30, no. 4, p. 644-660.

_____, 1973, Total-field resistivity mapping: Resumes of the 43rd Annual Meeting of the Society of Exploration Geophysicists, October, 1973, p. 50.

Appendix A

The following quantities for the dipole mapping survey are listed:

N	Station number
R1	Distance from observation point to one end of the source dipole, measured in miles
R2	Distance from observation point to the other end of the dipole source, measured in miles
D	The angle between the two lines R1 and R2 running from an observation point to the two ends of the source dipole
T	The angle between the two directions in which electric field measurements were made at each site, nominally 90 degrees
V1	Voltage measured between one pair of receiver electrodes, in microvolts
V2	Voltage measured between the other pair of receiver electrodes, in microvolts
L	Length of receiver dipole, in meters
I	Amplitude of current steps, in amperes
RA	Apparent resistivity calculated assuming spherical spreading of current in a uniform earth, in ohm-m
SA	Apparent conductance calculated assuming cylindrical spreading of current in a uniform conducting plate, in mhos

N	R1	R2	D	T	V1	V2	L	I	RA	SA
1	0.65	1.91	16	92	780	310	91.5	24.0	2.99	267.
2	1.04	2.31	8	95	570	100	91.5	24.0	5.90	198.
3	1.42	2.70	6	88	180	40	91.5	24.0	3.77	401.
4	1.82	3.10	4	94	110	0	91.5	23.0	4.30	432.
5	2.21	3.50	3	95	40	0	91.5	23.0	2.52	871.
6	0.57	1.65	43	94	540	200	91.5	23.0	1.62	485.
7	0.93	1.87	40	89	100	60	91.5	23.0	0.94	1348.
8	1.28	2.06	37	91	100	80	91.5	23.0	2.24	790.
9	1.75	2.37	33	94	110	60	91.5	23.0	4.94	510.
10	2.20	2.70	28	91	140	60	91.5	23.0	11.07	293.
11	2.59	3.02	25	90	70	60	91.5	28.0	8.61	452.
12	2.98	3.38	22	93	80	0	91.5	28.0	11.21	400.
13	3.31	3.73	20	94	40	0	91.5	23.0	9.08	542.
14	3.80	4.23	18	92	20	0	91.5	23.0	6.56	857.
15	1.38	2.34	28	88	120	110	91.5	23.0	3.31	522.
16	2.16	2.85	25	91	100	100	91.5	23.0	9.57	303.
17	0.38	1.32	76	90	4000	560	91.5	23.0	4.58	132.
18	0.77	1.37	68	93	360	220	91.5	23.0	2.13	592.
19	1.52	1.79	42	92	110	100	91.5	23.0	4.04	613.
20	1.62	1.68	47	90	150	100	91.5	23.0	4.74	559.
21	0.45	1.72	11	91	1500	150	91.5	23.0	2.53	228.
22	0.78	0.86	104	103	820	540	91.5	23.0	3.61	363.
23	0.93	1.27	70	88	600	260	91.5	23.0	4.50	353.
24	1.25	1.80	46	97	330	240	91.5	24.0	6.70	288.
25	1.57	2.10	38	108	440	80	91.5	24.0	13.75	172.

N	R1	R2	D	T	V1	V2	L	I	RA	SA
26	2.08	2.59	30	97	110	50	91.5	24.0	7.45	414.
27	2.25	2.91	25	93	30	30	91.5	23.0	3.26	941.
28	2.45	3.29	20	102	30	0	91.5	23.0	2.76	1091.
29	1.94	2.75	25	86	60	20	91.5	23.0	3.07	809.
30	1.57	2.47	27	91	120	0	91.5	23.0	3.44	575.
31	1.14	2.09	32	112	150	110	91.5	23.0	3.07	478.
32	0.85	1.64	52	101	320	120	91.5	23.0	2.39	527.
33	0.67	1.77	36	82	700	250	91.5	23.0	2.80	316.
34	2.21	2.40	32	82	90	60	91.5	28.0	5.97	601.
35	1.81	2.06	39	85	110	0	91.5	23.0	4.45	663.
36	1.08	1.66	51	90	310	100	91.5	23.0	3.65	460.
37	1.03	1.30	66	91	380	150	91.5	23.0	3.59	437.
38	2.39	2.43	31	92	140	40	91.5	28.0	10.13	382.
39	2.37	2.61	30	38	250	220	91.5	28.0	17.99	212.
40	2.72	2.89	26	45	100	50	91.5	28.0	11.18	393.
41	3.57	3.86	20	44	50	40	91.5	23.0	14.09	396.
42	3.57	3.72	20	91	20	0	91.5	23.0	5.76	997.
43	3.17	3.30	23	90	60	0	91.5	23.0	11.95	429.
44	2.76	2.95	26	43	90	70	91.5	23.0	12.12	367.
45	3.49	3.51	21	89	20	0	91.5	23.0	5.20	1032.
46	3.10	3.24	23	95	60	0	91.5	23.0	11.46	437.
47	2.84	3.17	24	96	30	0	91.5	23.0	4.46	988.
48	3.48	3.61	21	87	20	0	91.5	23.0	5.24	1073.
49	2.43	2.85	26	91	90	70	91.5	23.0	11.86	321.